Thin-Walled Structures 95 (2015) 221–230

Contents lists available at ScienceDirect

Thin-Walled Structures

journal homepage: www.elsevier.com/locate/tws

Fundamental behaviour of concrete-filled pentagonal flange plate girders under shear

M.F. Hassanein *

Department of Structural Engineering, Faculty of Engineering, Tanta University, Tanta, Egypt

ARTICLE INFO

Article history:
Received 30 January 2015
Received in revised form
19 June 2015
Accepted 3 July 2015
Available online 18 July 2015

Keywords:
Concrete-filled pentagonal flange plate girder
Shear failure mechanism
Web panel
Transversal stiffener
Finite element analysis
Ultimate capacity
Structural design.

ABSTRACT

Hollow tubular flange plate girders are found to possess higher flexural and shear strengths over those of I-section plate girders with flat flanges. Recently, concrete-filled pentagonal flange girders (CFPFGs) have been suggested in literature to increase the out-of-plane flexural strength of the girders. The geometrical configuration of the section is assumed identical to that of the girder with the rectangular concrete-filled flanges, but the flange depth-to-width ratio is designed to be larger in order to reduce the local buckling of the web. In this paper, the fundamental shear behaviour of these CFPFGs with slender stiffened webs is investigated. Nonlinear three-dimensional finite element (FE) analyses using ABAQUS are employed to conduct parametric studies, having first validated the models against available experimental data. For comparison purposes and to examine the effect of the infill concrete, steel pentagonal flange girders (SPTGs) are also generated. It is found that CFPFGs and SPFGs with the same dimensions have similar buckling shapes but with different loads with the buckling load of the CFPFG being higher than that of the corresponding SPFG. In the post-buckling stage, the width of the inclined tension field becomes greater in the CFPFGs relative to that of the SPFGs. This highlights the influence of the infill concrete which increases the stiffness of the upper flanges, and hence allows the webs to carry additional shear loads compared to SPFGs. Several affecting parameters are, additionally, examined and important conclusions are remarked. The FE strengths are compared with the design strength of the webs following the EN 1993-1-5, indicating that it can conservatively be used with the SFPGs. On the other hand, it becomes highly conservative for the CFPFGs.

1. Introduction

Girders, in practice, are subjected to significant levels of bending moment and thus failure typically occurs when the applied moment at the critical section exceeds its flexural capacity. Therefore, girders, in conventional design, are typically designed to satisfy the flexural limit state, controlled by the flexural-torsional buckling or by the propagation of plastic hinges, and then they are checked for the shear limiting criteria. To increase the flexural-torsional buckling strength of I-section plate girders with flat flanges (IPGs) several solutions may be applied, such as reducing their unbraced lengths, increasing the dimensions of their flanges or recently by replacing the flat flanges by hollow tubular flanges [1–6]. By using hollow tubular flanges, the vertical dimension of the tube reduces the depth of the web, overcoming problems with web slenderness design limits. Nevertheless, the web panel of plate girders with slender webs buckles at a relatively low value of the applied load, at which the shear may control the design. To overcome the shear strength reduction associated with utilizing plate girders with slender webs in construction, the webs are often reinforced with transversal stiffeners along their spans. Overall, it was found that using the hollow tubular flange plate girders instead of IPGs is a powerful tool not only to increase the flexural strength of the girders, but also to provide higher shear strengths [7,8].

On the other hand, using concrete-filled steel tubular (CFST) members in structures and bridges has been increased in recent decades, due to their excellent structural performance characteristics including high strength, stiffness as well as high ductility; see for example [9,10]. Hence, several researches investigated bridges with concrete-filled tubular flange girders (CFTFGs) [11–14]. Typical examples of the CFTFGs are shown in Fig. 2(a) and (b). Wimer and Sause [12] investigated the CFTFGs with rectangular CFST as the compression flange (Fig. 2(a)), while Kim and Sause [13,14] examined those with round CFSTs (Fig. 2(b)). Generally, it was found that CFTFGs provide more strength, stiffness and stability than IPGs with flat plate flanges with the same amount of

* Fax: +20403315860.
E-mail addresses: mostafa.fahmi@yahoo.com, mostafa.fahmi@f-eng.tanta.edu.eg

http://dx.doi.org/10.1016/j.tws.2015.07.003
0263-8231/

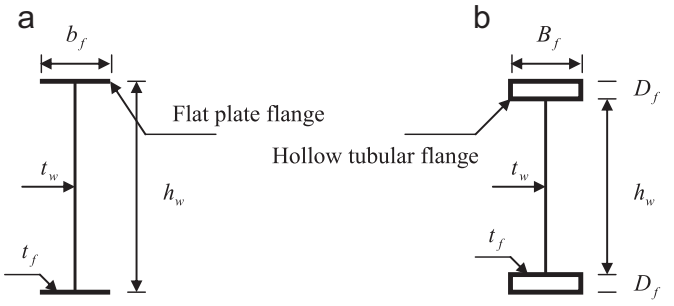

Fig 1. Typical plate girders.

steel [12–14]. It was, as well, found that the large torsional stiffness of the tubular flanges permits the use of large unbraced lengths in bridge framing systems. More recently, Gao et al. [15] investigated experimentally and numerically the flexural behaviour of the girder shown in Fig. 2(c) which is called the concrete-filled pentagonal flange beam. The cross-section of an I-section beam was modified by welding an additional steel plate (drawn by dashed lines in Fig. 2(c)) to its top flange to form an upper box flange section filled with concrete. The geometrical configuration of the section was, however, assumed by Gao et al. [15] identical to that of the CFTFGs with the rectangular CFST but the flange depth-to-width ratio was designed to be larger *in order to reduce the tendency of web local buckling*.

To widen the use of the concrete-filled pentagonal flange girder (CFPFG) with its numerous structural benefits (Fig. 2(c)), it is investigated in this paper for its shear behaviour. To the author's best knowledge, this has never been carried out in literature. Nonlinear three-dimensional finite element (FE) analyses using ABAQUS [16] are employed to conduct parametric studies, having first validated the models against available experimental data [15]. Girders with slender stiffened webs are currently considered. Several affecting parameters are examined and important conclusions are remarked.

2. FE model and validation

The nonlinear FE analysis program ABAQUS/Standard [16] was used to investigate the shear behaviour of simply supported CFPFGs, taking into account the geometrical and material nonlinearities. For nonlinear analyses, geometric imperfection should be considered in the FE model, by performing elastic buckling analysis first on a perfect beam to obtain its buckling mode. The material plasticity strains and geometric imperfections, based on the first positive eigenmode, should then be included in the second step of the nonlinear analysis (Riks method) to obtain the ultimate loads as well as the failure modes of the CFPFGs. The

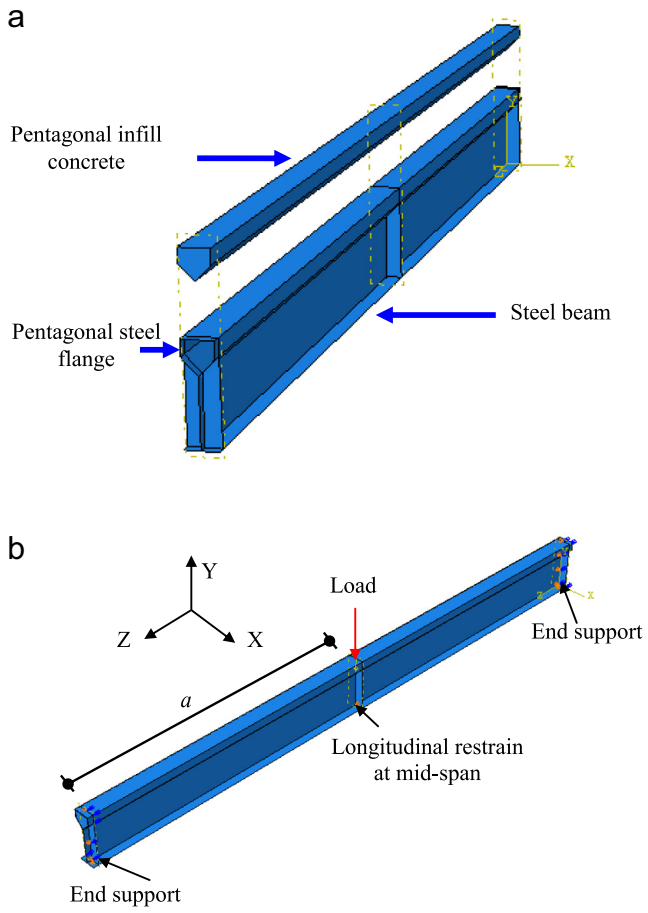

Fig. 3. Typical FE model for tested CFPFBs. (a) Components and (b) load and boundary conditions.

measured initial imperfection value of $L/1000$ is used in the FE models simulating the experimental tests [15].

2.1. General

A typical FE model for the CFPFB is shown in Fig. 3. As can be seen from Fig. 3(a), the CFPFG is composed of two main parts; the infill pentagonal concrete and the steel girder with suitable interactions between them. The pentagonal steel tubes shown in Fig. 2(c) are formed from a flat flange plate and a cold-formed section which is in turn divided into flat and corner zones. To simulate the bond between the pentagonal steel tube and the infill concrete, surface-based interactions with a contact pressure-

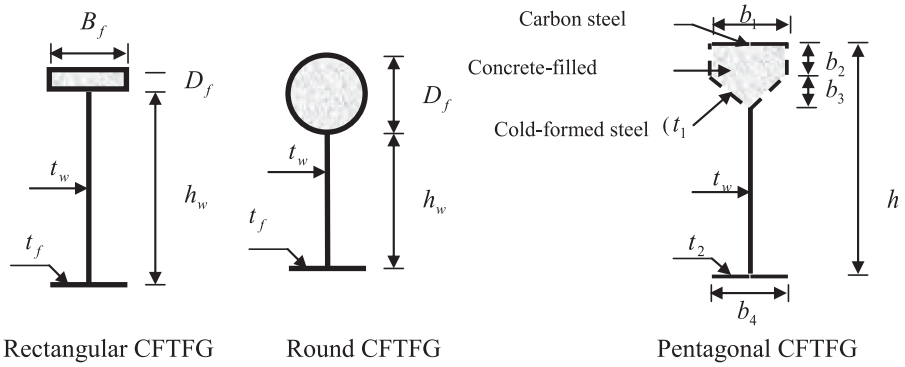

Fig 2. Typical concrete-filled tubular flanges girders (CFTFGs).

overclosure model in the normal direction and a Coulomb friction model in the longitudinal direction were employed. The steel surfaces were chosen as slave surfaces whereas the infill concrete surfaces were treated as the master. The friction coefficient between the pentagonal steel tube walls and the infill concrete was taken as 0.4.

Simply supported boundary conditions were applied to end sections. At each end section, the twist rotation about z-axis of all nodes of the section was restrained (ϕ_z=0.0). The lateral displacement in x-axis of all nodes on the y-axis (at x=0.0) was restrained (u_x=0.0). The vertical displacement of the web was restrained (u_y=0.0), while the longitudinal displacement in z-axis of a centre point at the lower flange was restrained (u_z=0.0). The vertical concentrated load was applied in the mid-span as shown in Fig. 3(b). To prevent the flexural-torsional buckling, lateral displacements were restrained at the loaded mid-span points. The load was applied incrementally using the modified Riks method [16]. The nonlinear geometry parameter (*NLGEOM) was included to allow for changes in geometry under load. The steel material was assumed to behave in an elastic-perfectly plastic manner.

The concrete part was meshed with the solid element known as C3D8R [16]. This element type is an 8-node brick element with reduced integration stiffness. Each node has three translational degrees of freedom. This element can be used for nonlinear analysis including contact, large deformation, plasticity and failure. The steel beam and the stiffeners were modelled in the same part and meshed with shell element (S4R). S4R element has six degrees of freedom per node, providing accurate solution to most applications and allows for transverse shear deformation. The element also accounts for finite strain and is suitable for large strain analysis. Simpson rule with five integration points was used through the included element thickness. The mesh sensitivity analyses were conducted to find the appropriate mesh size. They indicated that overall mesh size of 20 mm is accurately presenting the behaviour of the current girders with good solution timing. The FE mesh of a typical tested specimen is presented in Fig. 4.

2.2. Stress–strain relationships of the materials

2.2.1. Structural steel material model

Structural steel elements were modelled in the nonlinear analysis as a bilinear elastic–plastic stress–strain curve with linear strain hardening, as can be seen in Fig. 5. In the linear elastic part of the curve, Young's modulus (E_0) and Poison's ratio of 210 GPa and 0.3, respectively, were used. In the hardening part of the curve, a Modulus of E_0/100 was used. This ignores the effect of the cold-formed steel used in the flanges of the verified pentagonal girders according to pre-analysis on its effect.

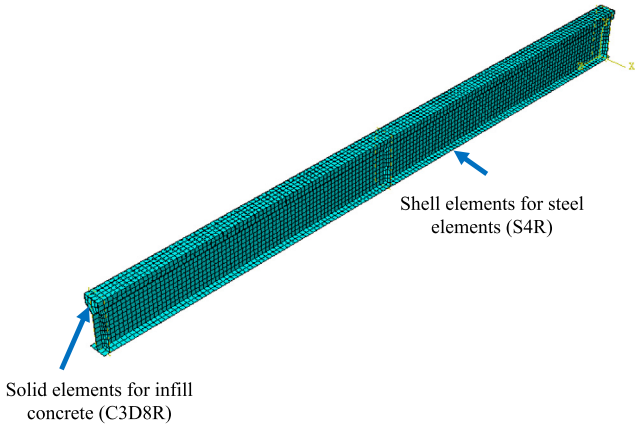

Fig. 4. Typical FE mesh for CFPFBs' components.

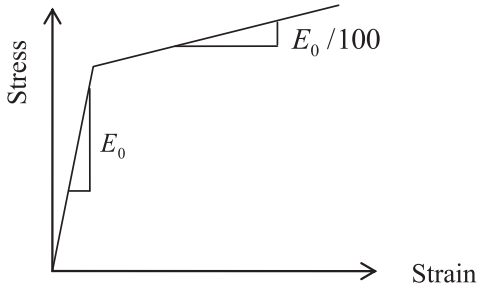

Fig. 5. Bilinear stress–strain curve adopted for steel elements.

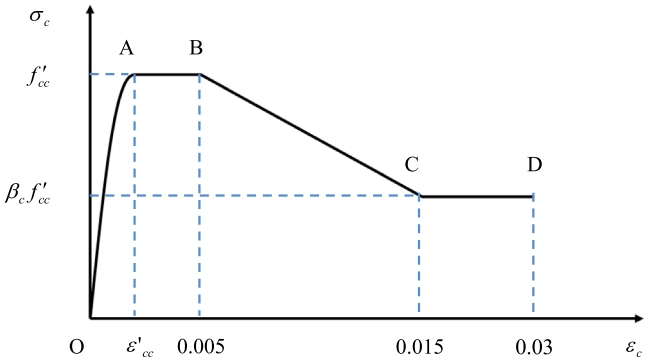

Fig. 6. Stress–strain curve for the confined concrete in CFPFGs.

2.2.2. Infill concrete material model

The infill concrete in CFPFGs subjected to transverse loading acts mainly as a compression member. Hence, the elastic–plastic material behaviour of the confined concrete in rectangular CFST columns, shown in Fig. 6, was used. The pentagonal flange was assumed as a rectangular CFST column with width and depth dimensions of b_1 and b_2+b_3, respectively. Experiments indicate that the confinement effect provided by rectangular steel tubes increases mainly the ductility of the concrete core in short CFST columns but not their ultimate strengths. [17]. The part OA of the stress–strain curve (Fig. 6) is represented using the equations suggested by Mander et al. [17] as

$$\sigma_c = \frac{f`_{cc}\lambda(\varepsilon_c/\varepsilon`_{cc})}{\lambda - 1.0 + (\varepsilon_c/\varepsilon`_{cc})^{\lambda}} \quad (1)$$

$$\lambda = \frac{E_c}{E_c - (f`_{cc}/\varepsilon`_{cc})} \quad (2)$$

where σ_c is the longitudinal compressive concrete stress, f'_{cc} is the effective compressive strength of confined concrete, ε_c is the longitudinal compressive concrete strain, ε'_{cc} is the strain at f'_{cc} and E_c is the Young's modulus of concrete which is given by ACI [18] as

$$E_c = 3320\sqrt{f`_{cc}} + 6900(\text{MPa}) \quad (3)$$

$$\varepsilon`_{cc} = \begin{cases} 0.002 & \text{for } f`_{cc} \le 28(\text{MPa}) \\ 0.002 + \dfrac{f`_{cc} - 28}{54000} & \text{for } 28 < f`_{cc} \le 82(\text{MPa}) \\ 0.003 & \text{for } f`_{cc} > 82(\text{MPa}) \end{cases} \quad (4)$$

The parts AB, BC and CD of the stress–strain curve for confined concrete depicted in Fig. 6 are based on the model given by Tomii and Sakino [19] and are defined as

$$\sigma_c = \begin{cases} f'_{cc} & \text{for: } \varepsilon'_{cc} < \varepsilon_c \le 0.005 \\ \beta_c f'_{cc} + 100(0.015 - \varepsilon_c)(f'_{cc} - \beta_c f'_{cc}) & \text{for: } 0.005 < \varepsilon_c \le 0.015 \\ \beta_c f'_{cc} & \text{for: } \varepsilon_c > 0.015 \end{cases} \quad (5)$$

where β_c reflects the confinement effect on the concrete ductility and it depends on the width-to-thickness ratio (B_s/t) of the concrete-filled pentagonal flange, where B_s is taken as the larger depth of the rectangular flange cross-section. Based on the experimental results presented by Tomii and Sakino [19], β_c is proposed as:

$$\beta_c = \begin{cases} 1.0 & \text{for: } \frac{B_s}{t} \le 24 \\ 1.5 - \frac{1}{48}\frac{B_s}{t} & \text{for: } 24 < \frac{B_s}{t} \le 48 \\ 0.5 & \text{for: } \frac{B_s}{t} > 48 \end{cases} \quad (6)$$

The effective compressive strength of concrete (f'_{cc}) is influenced mainly by the column size, the quality of concrete and the loading rates on the concrete compressive strength. Hence, the value of $f'_{cc}$was modified using the strength reduction factor γ_c [20] as

$$\gamma_c = 1.85 D_c^{-0.135} \quad (7)$$

where D_c is the depth of the concrete.

The softening behaviour of concrete in the post-yield stage is determined by the parameter β_c and concrete strain ε_{cu}. The parameter β_c given in Eq. (6) accounts for the effect of B_s/t ratio of the steel tube on the softening of the concrete. The concrete strain ε_{cu} is taken as 0.03. The "Concrete Damaged Plasticity" model was applied to describe the constitutive behaviour of the infill concrete. To represent the inelastic behaviour of concrete, this model uses the concept of isotropic damaged elasticity, in combination with isotropic tensile and compressive plasticity. The model assumes that the uniaxial tensile and compressive responses of concrete are characterized by damaged plasticity. The plasticity parameters required by the "Concrete Damaged Plasticity" model [16] are the dilation angle, the eccentricity, the ratio of the strength in the triaxial state to that in the uniaxial state and the K parameter. They were taken, correspondingly, as 20°, 0.1, 1.16 and 0.667 [21,22].

The current model also accounts for the tensile strength of concrete which was taken as $f_t = 0.6(\gamma_c f'_c)^{1/2}$; γ_c is given previously by Eq. (7) and f'_c is the unconfined compressive concrete strength. The concrete tensile softening behaviour was considered. The ultimate tensile strain of the concrete considering the tensile softening model is 10 times the strain at cracking [23].

2.3. Validation of the FE model

To assess the accuracy of the generated FE models, the tests conducted by Gao, et al. [15] were simulated herein. Details of the tests were given previously in Table 1. Two specimens of CFPFB with and without transverse stiffener under the load (denoted separately by BWS and BWTS) were tested to failure [15]. 3 mm thick steel flat plates were used as transverse stiffeners which were welded to the flanges and the web of the section. The average compressive strength of the concrete cubes after 28 days was 59.2 N/mm^2. The geometrical and material properties of the CFPFB specimens are given in Tables 1 and 2, respectively, at which the definition of symbols was given previously in Fig. 1(c). It is of great importance to note that all displacement transducers used in the tests were removed at the load levels of 70 kN and 65 kN for BWS and BWTS, respectively, for a safe operation. Hence, the displacement readings after the previously mentioned load levels were not recorded. The ultimate loads of the CFPFBs obtained from the FE analyses ($P_{ul,FE}$) are compared with the test strengths ($P_{ul,Exp}$) in Table 3. As can be seen, the FE model yields good predictions of the ultimate loads of the CFPFBs. The mean value of $P_{ul,FE}/P_{ul,Exp}$ is 1.05. However, the slight variation between the FE and experimental results is likely attributed to residual stress which was neglected in the FE simulation. Similar results were found by Gao, et al. [15]. Fig. 7 shows a comparison between the experimental and FE load-displacement curves. It can be seen from Fig. 7 that the FE model predicts well the initial stiffness and the strength of the CFPFBs until the load levels at which the displacement transducers were removed. However, the experimental vertical and lateral displacements in the case of BWS seem to be away from those captured by FE in the hardening stage. This is attributed to the fact that these displacements are inherently more variable and hence harder to predict accurately than ultimate strength due to the flat nature of the load-deformation response near the failure point specially in girders suffering from lateral-distortional buckling failure mode. As this is not the case of the models of the parametric study as the webs are stiffened and restrained to move outwards, this effect is believed to be avoided.

The deformed shapes at the ultimate loads of both CFPFBs are examined herein to thoroughly monitor the different failure modes. Typical to those observed experimentally [15], two failure modes were noticed in the FE results, which are lateral-distortional buckling (LD) and lateral-torsional buckling (LT). The former mode (i.e. LD buckling) dominated the failure of the girder BWTS, and is characterized by distinct twisting of the top (compressed) and bottom (tensioned) flanges, thus leading to web distortion; see Fig. 8(b). For the BWS, buckling takes place in lateral-torsional mode as the web becomes stiffened transversally at mid-span location, causing the lateral buckling to control, rather than the web distortions; see Fig. 9(b). Figs. 8 and 9 show the buckling modes (pictures in the left side) and failure modes (pictures in the right side) of the two tested girders. Obviously, the buckling modes have shapes with maximum unit displacement amplitude and no vertical deflection while the failure modes possess both the buckling mode shape and major axis vertical deflection. Overall, it can be

Table 2
Material properties of the components of the CFPFBs [15].

Element	Young's modulus (GPa)	Yield stress (MPa)	Tensile stress (MPa)
Steel web plate (3 mm)	200	317	486
Cold-formed steel (3 mm)	202	509	776
Steel flange plate (6 mm)	204	318	492

Table 1
Details of the tested CFPFB specimens [15].

CFPFB	b_1 [mm]	b_2 [mm]	b_3 [mm]	b_4 [mm]	t_1 [mm]	t_2 [mm]	t_w [mm]	h [mm]	L [mm]
BWTS/ BWS	80	40	40	80	3	6	3	250	2900

Table 3
Comparisons of numerical and experimental ultimate strengths.

CFPFB	P_{FE} [kN]	P_{Exp} [kN]	$(P_{FE})/(P_{Exp})$
BWTS	73.53	71.2	1.03
BWS	83.40	78.4	1.06

concluded that the developed FE model is reliable and suitable in predicting the behaviour and strength of CFPFBs, and therefore can be used to generate parametric studies.

3. Parametric study

3.1. Input data

In this section, nonlinear numerical simulations, based on the above verified FE model, are generated to provide new results on CFPFGs under shear loading. The girders were transversally stiffened each at a distance (a) of 725 or 1450 mm with double-sided flat plate stiffeners of a thickness equals 25.4 mm. For comparison purpose, FE models for steel pentagonal flange girders (SPFGs) were also generated. The properties of steel material of the current CFPFGs are similar to that tested experimentally by Gao et al. [15], while geometries were modified to allow for the shear failure mechanism to take place instead of the flexural failure seen in Figs. 8 and 9. The thickness of the lower flange was increased to 20 mm to raise the flexural capacity of the girders. The thickness of the plates forming the pentagonal flanges was kept fixed to 3 mm. In the generated models, the depth b_3 ranged from 10 to 40 mm and the web slenderness varied by changing the web depth (h_w) from 600 to 1000 mm. Different a/h_w ratios were additionally considered in the analysis. The maximum initial imperfection of $h_w/100$ allowed by the Bridge Welding Code [24], based on the first positive eigenmode as can be seen in Fig. 10 for the case of CFPFGs, was used in the parametric study; where h_w denotes the web-depth of the plate girders. The geometrical details of the models are given in Table 4. The ultimate load for each girder was determined from the results of the FE analysis. The ultimate shear strengths ($V_{ul,FE}$) were then determined as can be seen in

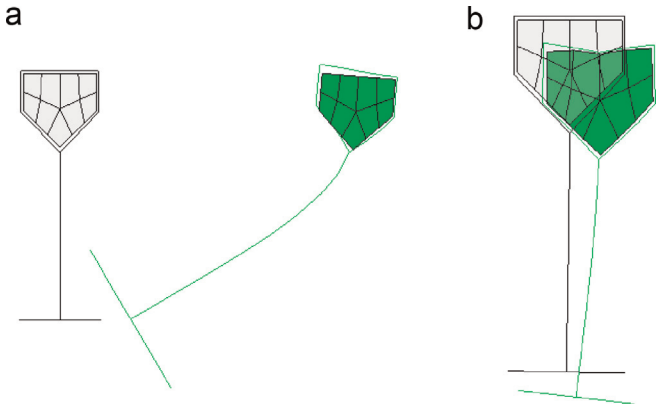

Fig. 8. Buckled/deformed and undeformed shapes at mid-span for BWTS.

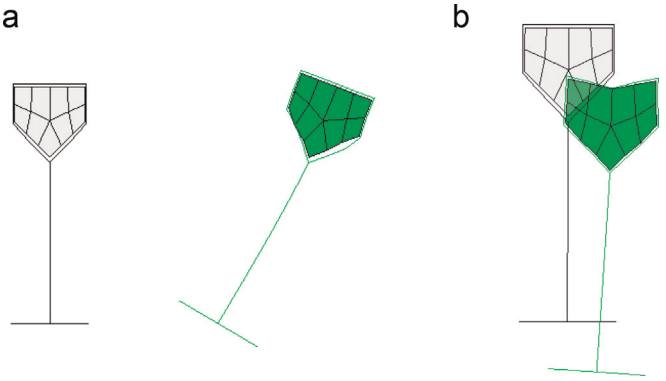

Fig. 9. Buckled/deformed and undeformed shapes at mid-span for BWS.

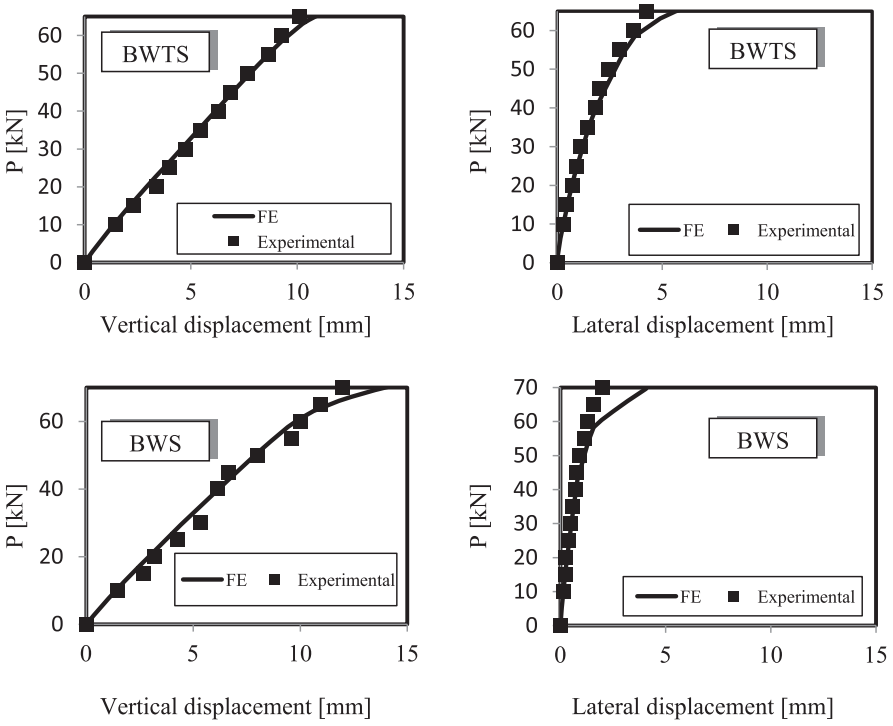

Fig. 7. Comparisons of FE and experimental load-displacement curves of CFPFB specimens.

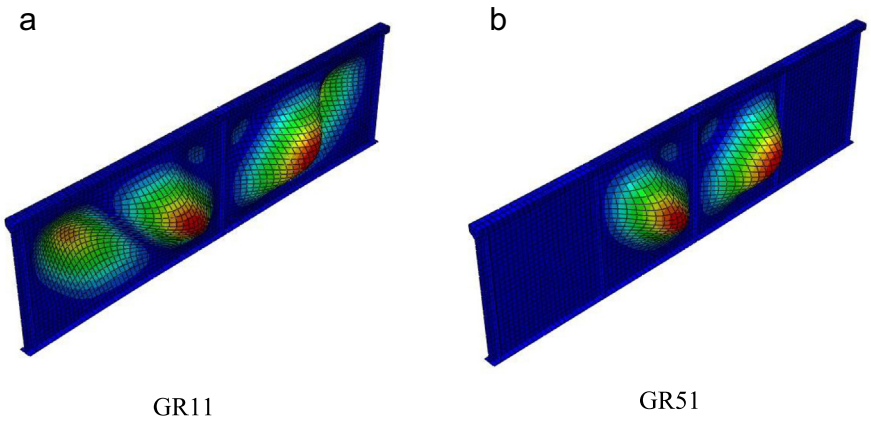

Fig. 10. Typical buckling modes for girders with different a/h_w ratios.

Table 4
Details and FE strengths of CFPFGs and SPFGs with $a=1450$ mm

Geometrical details			CFPFGs				SPFGs				[6]/[10]
h_w [mm] [1]	a/h_w [2]	b_3 [mm] [3]	Group [4]	Specimen [5]	$V_{ul,FE}$ [kN] [6]	$(V_{ul,FE})/(V_{w,pl})$ [7]	Group [8]	Specimen [9]	$V_{ul,FE}$ [kN] [10]	$(V_{ul,FE})/(V_{w,pl})$ [11]	[12]
600	2.42	10	G1	GR1	169	0.51	G6	GR21	155	0.47	1.09
		20		GR2	173	0.53		GR22	159	0.48	1.09
		30		GR3	178	0.54		GR23	164	0.5	1.09
		40		GR4	186	0.57		GR24	169	0.51	1.10
700	2.07	10	G2	GR5	193	0.5	G7	GR25	168	0.44	1.15
		20		GR6	199	0.52		GR26	174	0.45	1.14
		30		GR7	204	0.53		GR27	182	0.47	1.12
		40		GR8	213	0.55		GR28	188	0.49	1.13
800	1.81	10	G3	GR9	211	0.48	G8	GR29	186	0.42	1.13
		20		GR10	214	0.49		GR30	191	0.44	1.12
		30		GR11	224	0.51		GR31	199	0.45	1.13
		40		GR12	228	0.52		GR32	204	0.46	1.12
900	1.61	10	G4	GR13	229	0.46	G9	GR33	200	0.4	1.15
		20		GR14	233	0.47		GR34	205	0.41	1.14
		30		GR15	243	0.49		GR35	212	0.43	1.15
		40		GR16	255	0.52		GR36	217	0.44	1.18
1000	1.45	10	G5	GR17	246	0.45	G10	GR37	214	0.39	1.15
		20		GR18	252	0.46		GR38	219	0.4	1.15
		30		GR19	264	0.48		GR39	228	0.42	1.16
		40		GR20	276	0.5		GR40	233	0.42	1.18
Mean						**0.50**				**0.44**	**1.13**
Standard deviation						**0.032**				**0.034**	**0.027**

Tables 4 and 5 for girders with $a=1450mm$ and $a=725mm$, respectively. The plastic shear resistances of the webs ($V_{w,pl}$) were also calculated and the normalised shear strengths were given in the tables. It should be noted that girders of groups G1-G5 and G11-G15 were filled with concrete of $f'_c=60$ MPa. The effect of different concrete compressive strengths was also studied, as given in Section 3.5.

3.2. Structural behaviour

The CFPFGs and SPFGs failed in the current program by shear mechanism. Accordingly, the deformed shapes at the ultimate loads of the CFPFGs and SPFGs are examined herein to thoroughly monitor the difference in failure between both types of girders. Fig. 11 shows these deformed shapes for sample girders with $h_w=800$ mm and $b_3=30$ mm. Fig. 11(a) represents the deformed shapes of girders GR31 and GR11 characterised by $a/h_w=1.81$, while Fig. 11(b) provides girders GR71 and GR51 which had a/h_w ratio of 0.91. In both types of girders (CFPFGs and SPFGs), equal tensile and compressive principal stresses were found to develop in the web panel prior to buckling. Each pair of CFPFGs and SPFGs had similar buckling shapes (see Fig. 10) but with different loads with the buckling load of the CFPFG being higher than that of the corresponding SPFG. For the current examples, the buckling load of GR11 over that of GR31 is 1.18, while the buckling load of GR51 is 1.22 times that of GR71. In the post-buckling stage, an inclined tensile membrane stress state was developed as can be seen in Fig. 11. Once the web has yielded, failures of the both girders occur when plastic hinges are formed in the flanges. Obviously, the width of the inclined tension field becomes greater in the CFPFGs relative to that of the SPFGs. This highlights the influence of the infill concrete which increases the stiffness of the upper flanges, and hence allows the webs to carry additional shear loads compared to the SPFGs. It can be seen from Table 4 that the strength of GR11 over that of GR31 is 1.13 ($a/h_w=1.81$) which is smaller than the increase in the buckling load (1.18). In contrast, the increase in the strength of girders with smaller web panel aspect ratio (a/h_w) is much greater than the increase in the buckling load by adding the infill concrete; from Table 5 it is seen that the strength of GR51 over that of GR71 is 1.38 compared to 1.22 for the increase in the buckling load. From Tables 4 and 5 it can be seen that the average strength of the CFPFGs to that of the SPFGs are 1.13 and 1.35, respectively, for girders with $a=1450$ and 725 mm. Accordingly, it can be concluded that CFPFGs become much effective for girders with small a/h_w ratios.

Additional comparison that may represent the significance of

Table 5
Details and FE strengths of CFPFGs and SPFGs with $a=725$ mm.

Geometrical details			CFPFGs				SPFGs				[6]/[10]
h_w [mm] [1]	a/h_w [2]	b_3 [mm] [3]	Group [4]	Specimen [5]	$V_{ul,FE}$ [kN] [6]	$(V_{ul,FE})/(V_{w,pl})$ [7]	Group [8]	Specimen [9]	$V_{ul,FE}$ [kN] [10]	$(V_{ul,FE})/(V_{w,pl})$ [11]	[12]
600	1.21	10	G11	GR41	214	0.65	G16	GR61	164	0.5	1.30
		20		GR42	214	0.65		GR62	167	0.51	1.28
		30		GR43	221	0.67		GR63	172	0.52	1.28
		40		GR44	229	0.7		GR64	178	0.54	1.29
700	1.04	10	G12	GR45	245	0.64	G17	GR65	184	0.48	1.33
		20		GR46	245	0.64		GR66	185	0.48	1.32
		30		GR47	252	0.66		GR67	195	0.51	1.29
		40		GR48	263	0.68		GR68	201	0.52	1.31
800	0.91	10	G13	GR49	277	0.63	G18	GR69	205	0.47	1.35
		20		GR50	290	0.66		GR70	205	0.47	1.41
		30		GR51	292	0.67		GR71	212	0.48	1.38
		40		GR52	309	0.7		GR72	225	0.51	1.37
900	0.81	10	G14	GR53	294	0.6	G19	GR73	220	0.45	1.34
		20		GR54	306	0.62		GR74	226	0.46	1.35
		30		GR55	310	0.63		GR75	227	0.46	1.37
		40		GR56	316	0.64		GR76	228	0.46	1.39
1000	0.73	10	G15	GR57	312	0.57	G20	GR77	233	0.42	1.34
		20		GR58	321	0.58		GR78	233	0.42	1.38
		30		GR59	329	0.6		GR79	237	0.43	1.39
		40		GR60	353	0.64		GR80	240	0.44	1.47
Mean						**0.64**				**0.48**	**1.35**
Standard deviation						**0.035**				**0.035**	**0.049**

the infill concrete is to compare girders of groups G1-G5 (girders with infill concrete and $a=1450$) to their corresponding girders of groups G16-G20 (girders without infill concrete and $a=725$). The results show that a strength increase of about 6% in average (reached 15% in some cases) may be gained by reducing the number of stiffeners used and at the same time infilling the flange with concrete. Beside the strength increase, another benefits could be gained by reducing the number of stiffeners such as reducing the weld lines and the distortion caused by them.

3.3. *Effect of depth-to-width ratio of the pentagonal flanges*

The effect of the depth-to-width ratio of the pentagonal flanges is investigated in this sub-section through varying the depth (b_3), shown in Fig. 2, from 10 to 40 mm, while the width remained fixed to 80 mm. From the economical point of view, the optimization of the steel quantity (weight) becomes a relevant issue. Thus, it becomes important to evaluate the additional shear force carried by the CFPFGs and SPFGs compared with the increased amount of

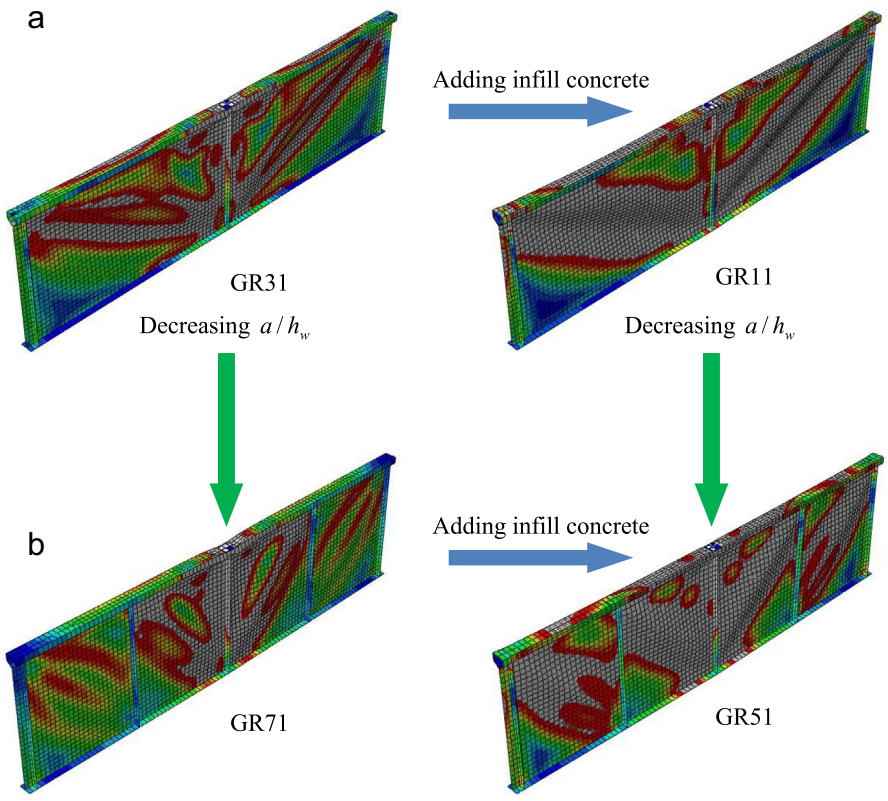

Fig. 11. Typical deformed shapes for girders with (a) $a/h_w=1.81$ and (b) $a/h_w=0.91$.

Table 6
Variation of cross-section area A (a_{ij}) and ultimate-to-plastic shear ratio $\chi=V_{ul,FE}/V_{w,pl}$ (c_{ij}) with b_3

h_w [mm]	b_3 [mm]	A [mm^2]	a_{ij}	c_{ij} $a/h_w=2.42$ ($a=1450$)		$a/h_w=1.21$ ($a=725$)	
Group				CFPFG G1	SPFG G6	CFPFG G11	SPFG G16
600	10	4127	0.00	0.00	0.00	0.00	0.00
	20	4148	0.01	0.02	0.03	0.00	0.02
	30	4180	0.01	0.05	0.05	0.03	0.04
	40	4219	0.02	0.09	0.08	0.06	0.08
Group				G5	G10	G15	G20
1000	10	5327	0.00	0.00	0.00	0.00	0.00
	20	5348	0.00	0.03	0.03	0.03	0.00
	30	5380	0.01	0.07	0.06	0.06	0.02
	40	5419	0.02	0.11	0.08	0.12	0.03

steel (proportional to the cross-section area) as a result of increasing the value of b_3. The percentage of variation of cross-section area (A) and ultimate-to-plastic shear ratio $\chi=V_{ul,FE}/V_{w,pl}$ between two girders (Gi and Gj) were calculated using the expressions:

$$a_{ij}=\frac{A_{Gi}-A_{Gj}}{A_{Gi}} \quad \text{and} \quad c_{ij}=\frac{\chi_{Gi}-\chi_{Gj}}{\chi_{Gi}} \tag{8}$$

The values of these coefficients are listed in Table 6 for sample results, at which it can be seen that the increase of the ultimate-to-plastic shear ratio (χ) is higher than the increase of cross-section area (A). Indeed, the increase in the cross-section area (A) by increasing b_3 is null. Although the increase in χ is noticed for the CFPFGs as well as the SPFGs with different web plate aspect ratios, it becomes noticeable for CFPFGs with large web depths. On the opposite, the effect of increasing b_3 is very small in SPFGs with closely spaced transversal stiffeners (i.e. $a=725$); see G20. Overall, it can be concluded that the plastic shear load carried by the girder increases more than the amount of steel. Hence, if the failure of the girder is related to the shear, the cross-section with the maximum possible b_3 is advantageous (economical) and should be used.

In order to illustrate the general behaviour of SPFGs as well as CFPFGs, the load-deflection curves of Groups G8 and G3 are plotted in Figs. 12 and 13, respectively. The curves of the SPFGs (G8) show an initially linear region before a gradual reduction in stiffness at $P_{ul,FE}$. After that, descending branches are exhibited. Obviously, the curves show that the increase in b_3 results in higher $P_{ul,FE}$ values. On the opposite, the CFPFGs (G3) show a typical rounded load-deflection curves without descending branches. The load-deflection curves tend to stop at the $P_{ul,FE}$ values due to FE

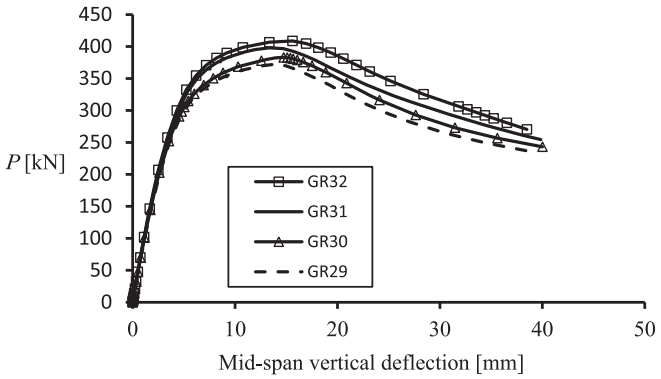

Fig. 12. Load-mid-span vertical deflection curves of G8.

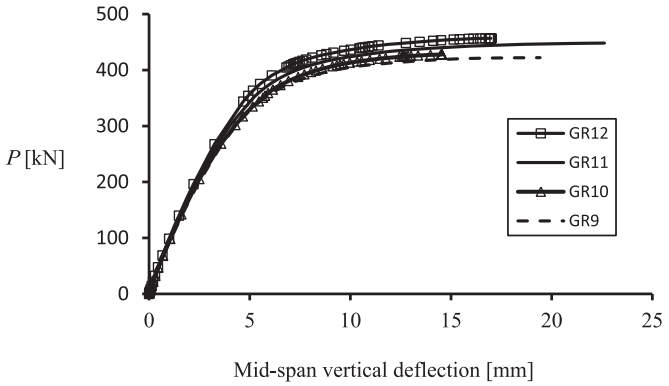

Fig. 13. Load-mid-span vertical deflection curves of G3.

convergence problems. However, the convergence problems, from the author's view point, do not affect the value of $P_{ul,FE}$ significantly as they happen after a long stabilised load-deflection behaviour.

3.4. Effect of aspect ratio of the web panel (a/h_w)

As previously noticed from Tables 4 and 5, decreasing the aspect ratio of the web panels (a/h_w) for the same girder geometries leads to the increase in the shear strength. Herein, the load-deflection curves for GR4 and GR44 are presented in Fig. 14 to illustrate the difference in their general behaviours. As can be seen, linear elastic behaviour appears for both girders from early loading stages. After that and until reaching the strength of the girders, a plastic plateau is shown for the girder with $a/h_w=2.42$, while the other with less a/h_w (i.e. 1.21) shows a strain-hardening response.

3.5. Effect of concrete compressive strength

The effect of the concrete compressive strength (f'_c) is investigated in this sub-section. In order to do so, GR6 and GR20 were remodelled considering different f'_c values ranging from 25 to 100 MPa, as can be seen in Table 7. From the table it can be seen that the value of f'_c has nearly slight effect on the strength of the CFPFGs, which could be ignored. The general behaviour of the girders as well did not show any difference. Hence, it can be concluded that the raised strength of the CFPFGs compared to that of the SPFGs is attributed to the availability of a rigid medium in the upper flange. Accordingly, the value of f'_c of the infill concrete should not be included in the design strength of the CFPFGs.

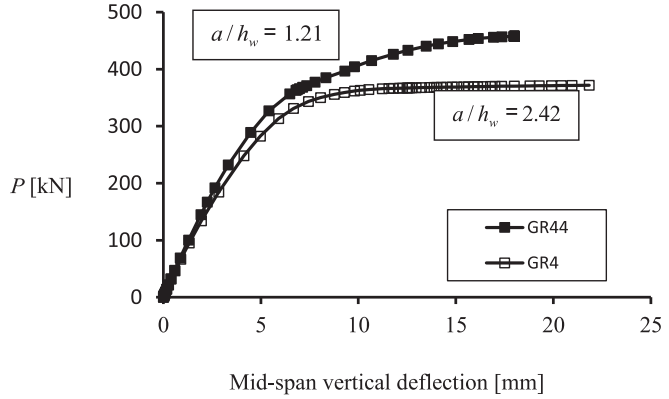

Fig. 14. Load-mid-span vertical deflection curves of GR4 and GR44.

Table 7
Details and FE strengths of the CFPFGs used to investigate the effect of f'_c.

Geometrical details h_w [mm] [1]	a/h_w [2]	b_3 [mm] [3]	CFPFGs Group [4]	Specimen [5]	f'_c [MPa] [6]	$V_{ul,FE}$ [kN] [7]	$(V_{ul,FE})/(V_{w,pl})$ [8]
700	2.07	20	G21	GR81	25	192	0.50
				GR82	40	196	0.51
				GR6	60	199	0.52
				GR83	80	200	0.52
				GR84	100	201	0.52
1000	1.45	40	G22	GR85	25	262	0.48
				GR86	40	267	0.49
				GR20	60	276	0.50
				GR87	80	277	0.50
				GR88	100	278	0.51
Mean							**0.50**
Standard deviation							**0.015**

3.6. Design strengths

According to the provisions of EC4 [25], the resistance to vertical shear should be taken as the resistance of the structural steel section unless the contribution from the infill concrete of the flange has been established. EN 1993-1-5 [26] provides the shear resistance just for the I-section plate girders, which is given here in Fig 1(a). According to EN 1993-1-5 [26], the design shear resistance $V_{b,Rd}$ should be taken as the lesser of the shear buckling resistance $V_{b,Rd}$ according to 5.2(1) of EN 1993-1-5 [26] and the plastic shear resistance ($V_{pl,Rd}$) according to 6.2.6(2) of EN 1993-1-1 [27]. Following clause 5.2(1) of EN 1993-1-5 [26], the design resistance for shear ($V_{b,Rd}$) for unstiffened or stiffened webs is taken as the sum of the shear carried by the web and the flanges. On

Table 8
Comparison between FE results and EN 1993-1-5 [26].

CFPFGs Group	Specimen	$V_{ul,FE}$ [kN]	$(V_{ul,FE})/(V_{EC3})$	SPFGs Group	Specimen	$V_{ul,FE}$ [kN]	$(V_{ul,FE})/(V_{EC3})$
G1	GR1	169	0.73	G6	GR21	155	0.67
	GR2	173	0.75		GR22	159	0.69
	GR3	178	0.77		GR23	164	0.71
	GR4	186	0.81		GR24	169	0.73
G2	GR5	193	0.95	G7	GR25	168	0.82
	GR6	199	0.98		GR26	174	0.85
	GR7	204	1.00		GR27	182	0.89
	GR8	213	1.05		GR28	188	0.92
G3	GR9	211	1.14	G8	GR29	186	1.01
	GR10	214	1.16		GR30	191	1.03
	GR11	224	1.21		GR31	199	1.08
	GR12	228	1.23		GR32	204	1.10
G4	GR13	229	1.34	G9	GR33	200	1.17
	GR14	233	1.37		GR34	205	1.20
	GR15	243	1.43		GR35	212	1.24
	GR16	255	1.50		GR36	217	1.27
G5	GR17	246	1.54	G10	GR37	214	1.34
	GR18	252	1.58		GR38	219	1.37
	GR19	264	1.66		GR39	228	1.43
	GR20	276	1.73		GR40	233	1.46
G11	GR41	214	1.49	G16	GR61	164	1.14
	GR42	214	1.49		GR62	167	1.16
	GR43	221	1.54		GR63	172	1.20
	GR44	229	1.59		GR64	178	1.24
G12	GR45	245	1.84	G17	GR65	184	1.38
	GR46	245	1.84		GR66	185	1.39
	GR47	252	1.89		GR67	195	1.46
	GR48	263	1.97		GR68	201	1.51
G13	GR49	277	2.23	G18	GR69	205	1.65
	GR50	290	2.33		GR70	205	1.65
	GR51	292	2.35		GR71	212	1.70
	GR52	309	2.48		GR72	225	1.81
G14	GR53	294	2.50	G19	GR73	220	1.87
	GR54	306	2.61		GR74	226	1.93
	GR55	310	2.64		GR75	227	1.93
	GR56	316	2.69		GR76	228	1.94
G15	GR57	312	2.78	G20	GR77	233	2.08
	GR58	321	2.86		GR78	233	2.08
	GR59	329	2.93		GR79	237	2.11
	GR60	353	3.15		GR80	240	2.14
Mean			**1.73**				**1.36**
Standard deviation			**0.687**				**0.432**

the opposite, AASHTO [28], AISC [29] and BS 5950-1:2000 [30] neglect the shear contribution from the flanges of the IPGs. Accordingly, the design strength carried merely by the webs [26] is compared to the FE strengths, as can be seen in Table 8, from which it can be seen that the strength of [26] can conservatively be used to predict the strength of the SFPGs (i.e. Mean of $V_{ul,FE}/V_{EC3}=1.36$). However, it would be highly conservative (i.e. Mean of $V_{ul,FE}/V_{EC3}=1.73$) if it is used for CFPFGs attributed to the considerable contribution of the infill concrete, as shown in the discussion. Overall, based on the absence of specific shear design strength formulae for the CFPFGs, a design model providing suitable capacity predictions for CFPFGs should be suggested. This will be provided in future publication containing parametric studies accounting for the contribution of the infill concrete of the upper pentagonal flange of the CFPFGs with *different flange sizes*, as suggested by EC4 [25].

4. Conclusions

Virtual tests were performed on concrete-filled pentagonal flange girders (CFPFGs) under shear loading by using ABAQUS [16]. The accuracy of the FE models were firstly assessed by using the experimental results of Gao et al. [15] and it was shown that the proposed model is able to predict well the general behaviour and strength. Then, parametric studies were performed considering the key affecting parameters which are the depth-to-width ratio of the pentagonal flanges, the web plate slenderness, the aspect ratio of the web panel and the compressive strengths of the infill concrete. Load displacement curves and failure modes were obtained from the analyses. For comparison purpose, steel pentagonal flange girders (SPFGs) were also generated. Based on this parametric study, the following points may be drawn:

1. Each pair of CFPFGs and SPFGs were found to have similar buckling shapes with the buckling load of the CFPFG being higher than that of the corresponding SPFG. The width of the inclined tension field, in the post-buckling stage, becomes greater in the CFPFGs relative to that of the SPFGs, highlighting the influence of the infill concrete which increases the stiffness of the upper flanges, and hence allows the webs to carry additional shear loads compared to the SPFGs.
2. The effect of the depth-to-width ratio of the pentagonal flanges was investigated through varying the depth (b_3). It was found that the cross-section with the maximum possible b_3 is advantageous (economical) and should be used. This is because it increases the ultimate-to-plastic shear ratio of the girder much higher than the increase in the cross-sectional areas.
3. It was clearly found that the decreasing the aspect ratio of the web panel (a/h_w) results in an increase in the shear strength of the girders. Such increase becomes greater in the CFPFGs compared to SPFGs.
4. It was shown that the concrete compressive strength (f'_c) has nearly no effect on the strength and behaviour of the CFPFGs. Hence, the raised strength of the CFPFGs compared to that of the SPFGs is attributed to the availability of a rigid concrete medium in the upper flange.
5. Through the comparison between the FE strengths and that calculated by EN 1993-1-5 [26], it was found that EN 1993-1-5 [26] can conservatively be used to predict the strength of the SFPGs. However, it becomes highly conservative if utilised for the CFPFGs due to the considerable contribution from the infill concrete.

Finally, based on the absence of specific shear design strength formulae for the CFPFGs, a design model providing suitable capacity predictions for CFPFGs should be suggested. This is underway by the current authors by considering additional parametric studies that account for the contribution of the infill concrete of *different pentagonal flange sizes*, as suggested by EC4 [25].

References

[1] J. Dong, R. Sause, Flexural strength of tubular flange girders, J. Constr. Steel Res. 65 (2009) 622–630.
[2] Y.L. Pi, N.S. Trahair, Lateral-Distorsional Buckling of Hollow Flange Beams, J. Struct. Eng., 123, ASCE (1997), p. 695–702.
[3] P. Avery, M. Mahendran, Finite-element analysis of hollow flange beams with web stiffeners, J. Struct. Eng. ASCE 123 (9) (1997) 1123–1129.
[4] M. Mahendran, D.P. Mahaarachchi, Development, behaviour and design of litesteel beam, in: Proceedings of the 4th International Symposium on Steel Structures, 2006, pp. 943–951.
[5] M.F. Hassanein, O.F. Kharoob, A.M. El Hadidy, Lateral-torsional buckling of hollow tubular flange plate girders with slender stiffened Webs, Thin-Walled Struct. 65 (2013) 49–61.
[6] M.F. Hassanein, N. Silvestre, Lateral-distortional buckling of hollow tubular flange plate girders with slender unstiffened webs, Eng. Struct. 56 (2013) 572–584.
[7] M.F. Hassanein, O.F. Kharoob, Shear strength and behavior of transversely stiffened tubular flange plate girders, Eng. Struct. 32 (9) (2010) 2617–2630.
[8] M.F. Hassanein, O.F. Kharoob, An extended evaluation for the shear behavior of hollow tubular flange plate girders, Thin-Walled Struct. 56 (2012) 88–102.
[9] N.E. Shanmugam, B. Lakshmi, State of the art report on steel-concrete composite columns, J. Constr. Steel Res. 57 (2001) 1041–1080.
[10] L.-H. Han, W. Li, R. Bjorhovde, Developments and advanced applications of concrete-filled steel tubular (CFST) structures: members, J. Constr. Steel Res. 100 (2014) 211–228.
[11] A. Smith, Design of HPS bridge girders with tubular flanges (M.S. thesis), Lehigh University, Bethlehem (PA, USA), 2001.
[12] M.R. Wimer, R. Sause, Rectangular tubular flange girders with corrugated and flat webs, ATLSS Report 04-18, ATLSS Engineering Research Center, Lehigh University, Bethlehem (PA, USA), 2004.
[13] B.G. Kim, R. Sause, High performance steel girders with tubular flanges, ATLSS Report 05-15, ATLSS Engineering Research Center, Lehigh University, Bethlehem (PA, USA), 2005.
[14] B.G. Kim, R. Sause, High performance steel girders with tubular flanges, Int. J. Steel Struct. 5 (3) (2005) 253–263.
[15] F. Gao, H.P. Zhu, D.H. Zhang, T.S. Fang, Experimental investigation on flexural behaviour of concrete-filled pentagonal flange beam under concentrated loading, Thin-Walled Struct. 84 (2014) 214–225.
[16] ABAQUS Standard User's Manual The Abaqus Software is a product of Dassault Systèmes Simulia Corp., Providence, RI, USA Dassault Systèmes, Version 6.8, USA, 2008.
[17] J.B. Mander, M.J.N. Priestley, R. Park, Theoretical stress–strain model for confined concrete, J. Struct. Eng., 114, ASCE (1988), p. 1804–1826.
[18] ACI-318, Building code requirements for reinforced concrete, ACI, Detroit (MI), 2002.
[19] M. Tomii, K. Sakino, Elastic–plastic behavior of concrete filled square steel tubular beam-columns, Trans. Architect. Inst. Jpn. 280 (1979) 111–120.
[20] Q.Q. Liang, Performance-based analysis of concrete-filled steel tubular beam-columns, Part I: theory and algorithms, J. Constr. Steel Res. 65 (2009) 363–372.
[21] M.F. Hassanein, O.F. Kharoob, Analysis of Circular Concrete-filled Double Skin Tubular Slender Columns with External Stainless Steel Tubes, Thin-Walled Struct. 79 (2014) 23–37.
[22] Z. Tao, Z.-B. Wang, Q. Yu, Finite element modelling of concrete-filled steel stub columns under axial compression, J. Constr. Steel Res. 89 (2013) 121–131.
[23] Q.Q. Liang, High strength circular concrete-filled steel tubular slender beam-columns, Part I: numerical analysis, J. Constr. Steel Res. 67 (2011) 164–171.
[24] AASHTO/AWS, Bridge welding code, ANSI/AASHTO/AWS D1.5M/D1.5:2002, A Joint Publication of American Association of State Highway and Transportation Officials, Inc., Washington, D.C., and American Welding Society, Miami, 2002.
[25] Eurocode 4, Design of Composite Steel and Concrete Structures-Part 1-1: General Rules and Rules for Buildings, British Standard Institution, CEN, 2004.
[26] EN 1993-1-5, Eurocode 3: Design of steel structures-Part 1-5: Plated structural elements, CEN, 2007.
[27] EN 1993-1-1, Eurocode 3: Design of steel structures-Part 1-1: General rules and rules for buildings, CEN, 2004.
[28] AASHTO, AASHTO LRFD Bridge Design Specifications (SI) (third edition), 2005.
[29] AISC, Load and Resistance Factor Design Specification, for Structural Steel Buildings, American Institute of Steel Construction, Chicago, 1999.
[30] BS 5950, Part 1: Code of Practice for Design-Rolled and Welded Sections, British Standard Institution, London, 2001.